

On the Directed Gas Phase Synthesis of the Imidoborane Molecule (HNBH) — An Isoelectronic Molecule of Acetylene (HCCH)

Fangtong Zhang, Pavlo Maksyutenko, and Ralf I. Kaiser*

University of Hawaii at Manoa, Department of Chemistry, Honolulu, Hawaii 96822, United States

Alexander M. Mebel

Department of Chemistry and Biochemistry, Florida International University, Miami, FL 33199

Adriana Gregušová, S. Ajith Perera, and Rodney J. Bartlett

Quantum Theory Project, University of Florida, Gainesville, FL 32611

Received: July 31, 2010; Revised Manuscript Received: October 7, 2010

The elementary reaction of ground state boron atoms, ($B(^2P_j)$), with ammonia ($NH_3(X^1A_1)$) was conducted under single collision conditions at a collision energy of $20.5 \pm 0.4 \text{ kJ mol}^{-1}$ in a crossed molecular beams machine. Combined with electronic structure calculations, our experimental results suggested that the reaction was initiated by a barrier-less addition of the boron atom to the nonbonding electron pair of the nitrogen atom forming a weakly bound BNH_3 collision complex. This intermediate underwent a hydrogen shift to a doublet $HBNH_2$ radical that decomposed via atomic hydrogen loss to at least the imidoborane ($HBNH(X^1\Sigma^+)$) molecule, an isoelectronic species of acetylene ($HCCH(X^1\Sigma_g^+)$). Our studies are also discussed in light of the isoelectronic C_2H_3 potential energy surface accessed via the isoelectronic carbon-methyl system.

1. Introduction

The linear imidoborane molecule (HNBH) has received considerable attention as a building block of the hetero aromatic borazine molecule ($B_3N_3H_6$) in a similar way as the isoelectronic acetylene species (HCCH) connects to the aromatic benzene molecule (C_6H_6) (Figure 1).^{1–3} Here, the dicarbon moiety (CC) of acetylene is formally replaced by an isolobal boron nitride unit (BN) to yield the imidoborane molecule. The isoelectronic properties are well reflected in similar bond distances of the boron–nitrogen and carbon–carbon triple bonds of 122 and 120 pm, respectively; the boron–hydrogen (117 pm) and nitrogen–hydrogen bond lengths (101 pm) are close to the carbon–hydrogen bond in acetylene (106 pm).⁴ The isolation of the imidoborane molecule, however, has eluded chemists for decades. Lory et al. detected imidoborane in a low temperature argon matrix upon photolysis of the ammonia–borane (H_3N-BH_3) precursor.⁵ More than 15 years later, Kawashima et al.⁶ recorded the gas phase infrared spectrum of transient imidoborane species in plasmas. In the most recent study, Andrews et al. followed the synthesis of imidoborane upon reaction of laser ablated boron atoms with ammonia in cryogenic matrices.^{7,8} The observation of the closed shell imidoborane (HNBH) and of the corresponding iminoborane radical (BNH) also triggered theoretical calculations on small hydrogenated boron–nitrogen clusters. Schleyer et al. suggested that the reaction of ground state boron atoms [$B(^2P)$] with ammonia leads to the formation of a weakly bound $B-NH_3$ complex, which isomerizes via a hydrogen shift to yield the $HBNH_2$ intermediate.⁹ On the other hand, Andrews et al. proposed an initial insertion of atomic boron of unknown electronic state into the nitrogen–hydrogen bond leading to the aminoborane, $HBNH_2$

intermediate. According to Schleyer et al., the $HBNH_2$ intermediate could isomerize to the thermodynamically less stable ($\sim 19 \text{ kJ mol}^{-1}$) borylamidogen radical (H_2BNH) or fragmented via atomic and molecular hydrogen losses to imidoborane (HNBH) and iminoborane (BNH), respectively. The C_{2v} symmetric aminoboranylidene (H_2NB) and borylnitrene (H_2BN) isomers were predicted to be higher in energy by $158–227 \text{ kJ mol}^{-1}$ ^{4,9,10} and $386–460 \text{ kJ mol}^{-1}$,^{4,10} respectively.

In this paper, we report on the very first “clean” synthesis of the imidoborane molecule utilizing the crossed molecular beam approach by crossing a supersonic beam of ground state boron atoms with a beam of ammonia molecules. This presents a prototype reaction of the simplest Lewis acids (the electron-deficient boron atom holds a 2P electronic ground state and a $(1s)^2(2s)^2(2p)^1$ electron configuration) with one of the simplest Lewis bases (the tetra atomic ammonia molecule). The experimental studies are contemplated with high level electronic structure calculations to compare the experimental findings with theoretical predictions to unravel the reaction mechanism(s).

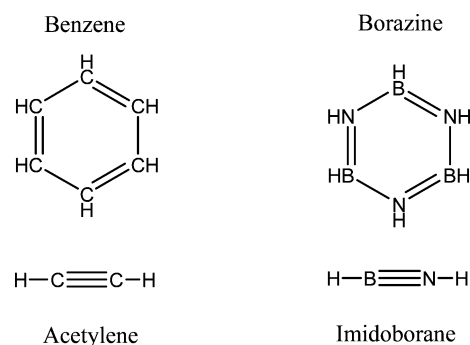


Figure 1. Structures of acetylene/benzene and imidoborane/borazine.

* To whom correspondence should be addressed. E-mail: ralfk@hawaii.edu.

This system is also of great interest from the physical organic and physical inorganic viewpoints since the BNH_3 and BNH_2 potential energy surfaces (PES) can be compared with the isoelectronic C_2H_3 and C_2H_2 benchmark systems.^{11–18}

2. Experimental Section

The elementary reaction of ground state boron atoms, $^{11}\text{B}(^2P_1)$, with ammonia, $\text{NH}_3(X^1A_1)$, was conducted in the gas phase under single collision conditions utilizing a universal crossed molecular beams machine at the University of Hawai'i. The experimental setup has been described in detail elsewhere.^{19–21} Briefly, a pulsed supersonic boron atom beam was generated in the primary source chamber by laser ablation of a boron rod at 266 nm (30 Hz; 5–10 mJ per pulse).¹⁹ The ablated species were seeded in neat helium carrier gas (99.9999%, Airgas) released by a Proch-Trickl pulsed valve at 4 atm backing pressure. It is important to stress that the boron beam is pulsed. Consequently, different parts of the boron beam have distinct peak velocities and speed ratios. To define the beam velocity and spread, a four-slot chopper wheel selected a part of the pulsed boron beam of a peak velocity, v_p , of $2200 \pm 20 \text{ ms}^{-1}$ and speed ratio of 3.6 ± 0.3 . This segment of the boron beam crossed a pulsed ammonia beam (99.9999%, Matheson Tri-Gas; 550 Torr) released by a second pulsed valve perpendicularly in the interaction region. The segment of the ammonia beam was defined by a peak velocity of $1140 \pm 30 \text{ ms}^{-1}$ and a speed ratio of 25.0 ± 0.5 . This gives to a collision energy of $20.5 \pm 0.4 \text{ kJ mol}^{-1}$ and a center-of-mass angle, Θ_{CM} , of $38.7 \pm 0.5^\circ$ with respect to ^{11}B . Note that the ablation beam contains both ^{11}B (80%) and ^{10}B (20%) in their nature abundances.

The experimental conditions (delay times, laser power, laser focus) were optimized so that the interference from higher boron clusters up to B_5 was minimized. Under normal circumstances, the minor contribution of higher boron clusters, which is less than 0.1%, does not interfere with the reactive scattering signal; however, in the present experiment, the reactive scattering signal at mass to charge, m/z , of 27 ($^{11}\text{BNH}_2$) (see Results) was very weak, and at angles closer to the primary beam, we have interference from doubly ionized, nonreactively scattered ($^{11}\text{B}_4^{10}\text{B}$)⁺² (hereafter B_5^{+2}). We would like to state explicitly that B_5^+ ($m/z = 54$) and B_5^{+2} ($m/z = 27$) were also detected at fractions of less than 0.1% in the primary beam on axis.

The scattered species were monitored using a quadrupole mass spectrometric detector in the time-of-flight (TOF) mode after electron-impact ionization of the molecules at 80 eV. This detector can be rotated within the plane defined by the primary and the secondary reactant beams to allow taking angular resolved TOF spectra. At each angle, up to 6×10^6 TOF spectra were accumulated to obtain good signal-to-noise ratios. The recorded TOF spectra were then integrated and normalized to extract the product angular distribution in the laboratory frame (LAB). To collect information on the scattering dynamics, the laboratory data were transformed into the center-of-mass reference frame utilizing a forward-convolution routine.^{22,23} This iterative method initially guesses the angular flux distribution, $T(\theta)$, and the translational energy flux distribution, $P(E_T)$ in the center-of-mass system (CM). Laboratory TOF spectra and the laboratory angular distributions (LAB) were then calculated from the $T(\theta)$ and $P(E_T)$ function and were averaged over a grid of Newton diagrams. Best fits were obtained by iteratively refining the adjustable parameters in the center-of-mass functions. The findings are compiled in a center-of-mass product flux contour map. This plot reports the differential cross section, $I(\theta, u)$, as a function of product center-of-mass scattering angle θ and

velocity u ; the flux contour plot is proportional to the product of the center-of-mass angular distribution, $T(\theta)$, and the center-of-mass velocity distribution, $P(u)$, which in turn is computed from the center-of-mass translational energy distribution, $P(E_T)$. The flux contour map, $I(\theta, u)$, can be seen as an image of the reaction and holds all the information of the reactive scattering process.

The primary beam was also characterized via laser induced fluorescence (LIF) to evaluate the population of the two spin-orbit states in ground state boron: $J = 1/2$ ($^2P_{1/2}$) and $J = 3/2$ ($^2P_{3/2}$, 15.254 cm^{-1}). The 5 μJ frequency-doubled output of Lambda Physik Scanmate dye laser saturated the $^2P-^2S$ transitions near 249.75 and 249.85 nm for $J = 1/2$ and $J = 3/2$, respectively. The interference filter centered at 250 nm with a 10 nm bandwidth placed in front of the photomultiplier tube (Hamamatsu, R955) discriminated against fluorescence on the surfaces inside the chamber. Sixteen detection laser shots were averaged for each point, step size was 0.001 nm. Four scans were averaged to produce the final spectrum. In saturation mode the ratio of state populations is inferred directly from the ratio of the line intensities. Statistics on the ratios for the four individual scans yield an average $J = 1/2$ to $J = 3/2$ ratio of 1.6 ± 0.2 corresponding to an electronic temperature $T = 18.5 \pm 2.0 \text{ K}$.

3. Theoretical Section

Geometries of the reactants, products, intermediates, and transition states in the B-NH_3 system were optimized using the coupled clusters CCSD(T,full) method with single and double excitations (CCSD), with perturbative treatment of triple excitations, and with all electrons taken into account in the calculations of electronic correlation.^{24–27} Dunning's correlation-consistent cc-pVTZ basis set²⁸ was used. Vibrational frequencies were computed at the same CCSD(T,full)/cc-pVTZ level of theory to confirm the character of stationary points on the PES as local minima (all real frequencies) or transition states (one imaginary frequency) and to obtain zero-point vibrational energy (ZPE) corrections. The final relative energies reported in the paper are thus computed at the CCSD(T,full)/cc-pVTZ + ZPE(CCSD(T,full)/cc-pVTZ) level. The calculations were carried out utilizing the ACES program package.²⁹ Some transition states were preliminary located using the hybrid density functional B3LYP/6-311G** method employing the GAUSSIAN 98 package.³⁰ Then, the B3LYP geometries were used as initial guesses for the CCSD(T,full)/cc-pVTZ optimization; it should be noted that the differences between the B3LYP and CCSD(T) geometries for these transition states appeared to be rather small. Ab initio calculations for the isoelectronic C-CH_3 system, described here for comparison, were carried out with geometry optimization at the B3LYP/6-311G** level and refinement of single-point energies using the CCSD(T)/CBS approach in which the coupled clusters calculations with Dunning's cc-pVDZ, cc-pVTZ, cc-pVQZ, and cc-pV5Z basis sets were followed by extrapolation of total energies to the complete basis set limit. The calculations for the C-CH_3 system were performed employing the Gaussian 98 and MOLPRO 2002³¹ codes.

4. Results

In our experiments, we detected reactive scattering signal at mass-to-charge, m/z , of 27, which corresponds to the formation of a molecule of the gross formula $^{11}\text{BNH}_2$ (Figure 1). Within the limits of our detection system, time-of-flight spectra (TOF) at $m/z = 26$ (^{11}BNH and $^{10}\text{BNH}_2$) are superimposable to those at $m/z = 27$. This finding has two significant implications: first,

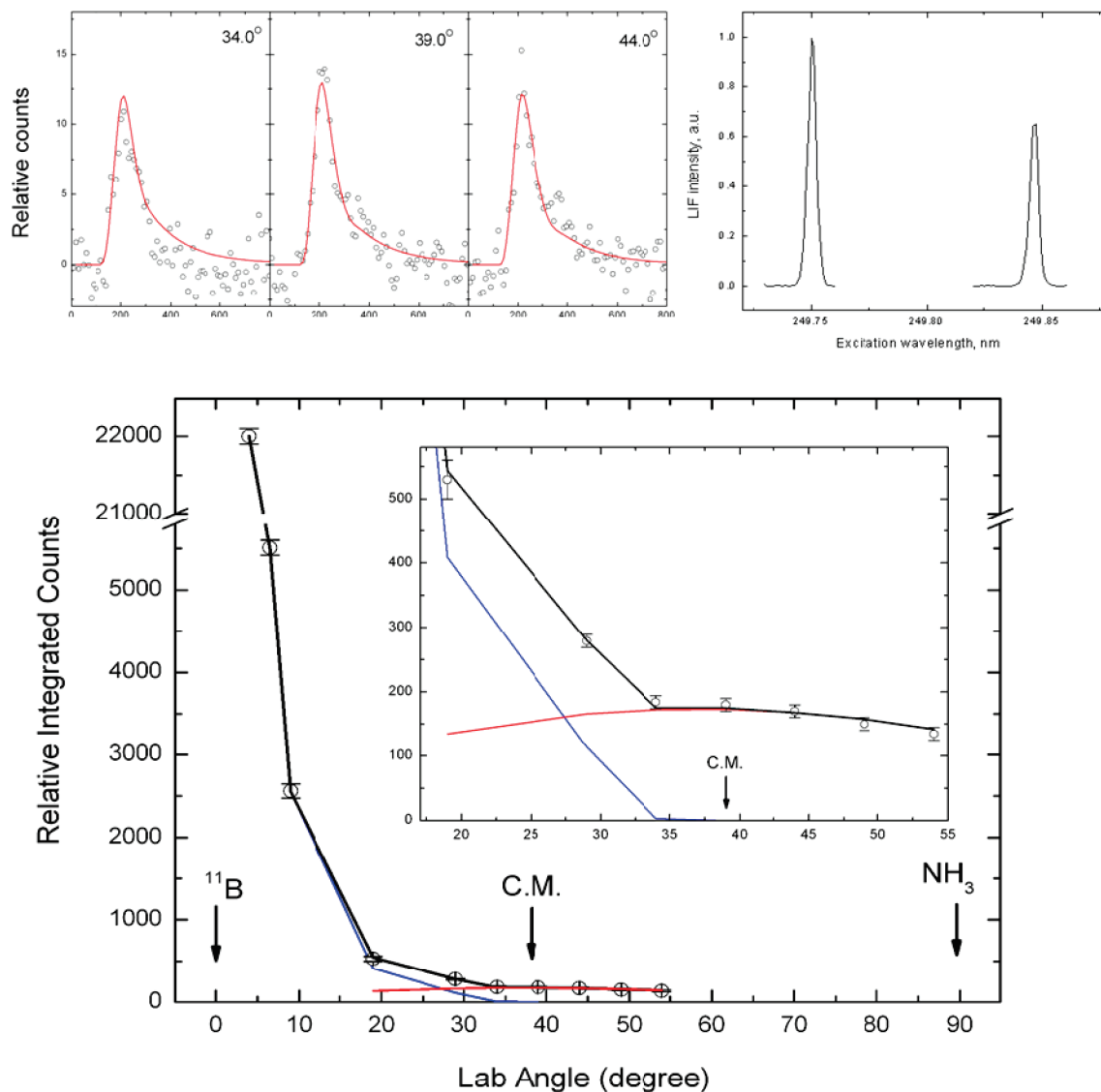


Figure 2. Top left: Time-of-flight data of reactive scattering signal at $m/z = 27$ (BNH_2^+) recorded for the reaction of atomic boron, $^{11}\text{B}(^2\text{P}_j)$, with ammonia $\text{NH}_3(\text{X}^1\text{A}_1)$ at various laboratory angles at a collision energy of 20.5 kJ mol^{-1} . The circles represent the experimental data, and the solid lines the fits. Each TOF spectrum has been normalized to the relative intensity at each angle. Top right: LIF spectrum of boron atom $^2\text{P}-^2\text{S}$ transitions near 249.75 and 249.85 nm for $J = 1/2$ and $J = 3/2$, respectively. Bottom: Laboratory angular distribution of the BNH_2^+ product recorded at $m/z = 27$ (BNH_2^+) at a collision energy of 20.5 kJ mol^{-1} for the reaction of atomic boron $^{11}\text{B}(^2\text{P}_j)$ with ammonia $\text{NH}_3(\text{X}^1\text{A}_1)$. Circles and error bars indicate experimental data, and the solid lines the calculated distributions with the best-fit center-of-mass functions. The red line represents the distribution obtained from the reactive scattering signal, whereas the blue line characterizes the inelastic scattering signal. The latter was fit by treating the scattering signal as a result of nonreactive scattering processes from a doubly charged boron cluster ($^{11}\text{B}_4^{10}\text{B}^{2+}$, $m/z = 27$) with ammonia.

within the sensitivity of our system, only the boron–hydrogen exchange pathway is open; second, under single collision conditions, we are forming a product of the formula $^{11}\text{BNH}_2$. For completeness, it should be mentioned that the reactive scattering signal was very weak; to obtain a reasonable signal-to-noise for the reactive signal, up to 6×10^6 TOF spectra had to be accumulated. Further, at angles closer to the primary beam, we had evidence of interference from nonreactive scattering signal at $m/z = 27$ scattered $^{11}\text{B}_4^{10}\text{B}^{2+}$ (hereafter B_5^{+2}) (see Experimental Section). Since this signal was found to diminish quickly once we moved away from the primary beam toward the center-of-mass angle of $38.7 \pm 0.5^\circ$, we were able to separate the contributions of nonreactively (from B_5^{+2}) from those of the reactively scattered signal at $m/z = 27$ (Figure 2). Since the goal of this paper is to untangle the formation of the imidoborane molecule, we will focus our subsequent discussion on the analysis of the reactive scattering signal.

A transformation of the TOF spectra and the corresponding angular distribution obtained at $m/z = 27$ from the laboratory to the center-of-mass reference frame helps to extract the underlying reaction dynamics, reaction energy, potential exit barriers, the nature of the reaction intermediates, and the mechanism(s) involved in the formation of distinct $^{11}\text{BNH}_2$ isomers under single collision conditions. Best fits of the reactive scattering signal and the TOF spectra as well as LAB distribution were achieved with only a single reactive channel as defined by the ^{11}B and NH_3 reactants and $^{11}\text{BNH}_2$ plus atomic hydrogen products. These fits resulted in only one center-of-mass translational energy distribution $P(E_T)$ and one angular distribution $T(\theta)$ (Figure 3). Let us investigate the center-of-mass energy distribution first. Here, the $P(E_T)$ extends to a maximum translational energy, E_{max} , of $300 \pm 20 \text{ kJ mol}^{-1}$. This limit denotes the sum of the collision energy plus the absolute of the reaction exoergicity. Therefore, E_{max} can be utilized to compute

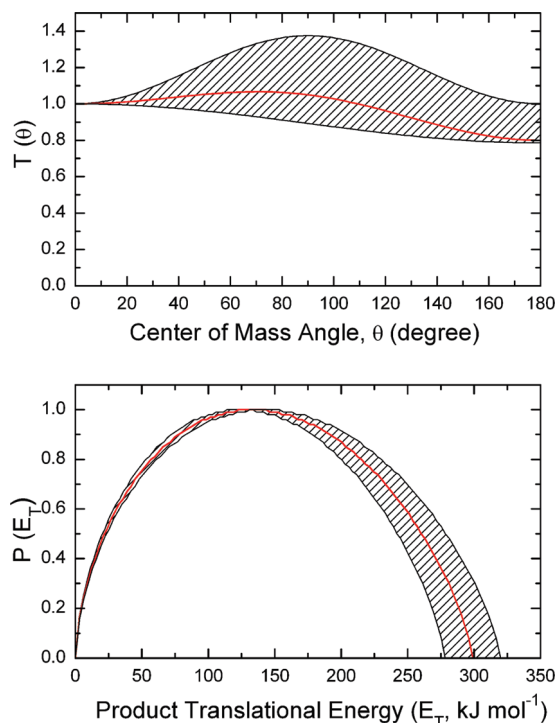


Figure 3. Center-of-mass angular (top) and translational energy flux distributions (bottom) of the reaction of atomic boron, $^{11}\text{B}(^2\text{P}_j)$, with ammonia, $\text{NH}_3(\text{X}^1\text{A}_1)$, at a collision energy of 20.5 kJ mol^{-1} for the BNH_2 product. Hatched areas indicate the acceptable upper and lower error limits of the fits. The red line defines the best fit functions.

the energetics of the reaction. Here, the reaction to form $^{11}\text{BNH}_2$ isomer(s) plus atomic hydrogen under single collision conditions is found to be exoergic by $280 \pm 20 \text{ kJ mol}^{-1}$. Further, the bell-like distribution holds a broad maximum at about $100\text{--}150 \text{ kJ mol}^{-1}$. In the most ideal case, this maximum could represent the existence of a tight exit transition state, when the intermediate complex decomposes to the final products;³² alternatively, this pattern likely indicates a weakly bound, short-lived intermediate similar to the CPH_3 intermediate formed in the reaction of ground state carbon atoms with phosphine.³³ Finally, the center-of-mass translational energy distribution also assists us to derive the fraction of total energy available channeling into the translational modes of the products. The averaged fraction of the available energy released into translation was

found to be $49 \pm 4\%$. This order of magnitude indicates that the intermediate could be rather short-lived; consequently, the energy randomization in the decomposing complex is not likely to be complete.³⁴

Besides the $P(E_T)$, the center of mass angular flux distribution, $T(\theta)$ also provides important information on the underlying reaction dynamics. Most importantly, the distribution depicts intensity over the complete angular range from 0 to 180° . This finding suggests that the reaction dynamics proceed via the formation of BNH_3 complex(es); these decompose via atomic hydrogen elimination to the BNH_2 product(s). Further, the best fit distribution is slightly forward-peaking, showing an intensity ratio at the poles of $T(0^\circ)/T(180^\circ) = 1.2 \pm 0.2$. This result suggests the existence of an osculating complex whose lifetime is comparable to the rotational period of the decomposing intermediate(s).³⁵ The forward-peaking requires that the attacking boron atom and the leaving hydrogen atom are located on opposite sides of the rotational axis.³⁶ Finally, the $T(\theta)$ also shows a mild side-way pattern; ratios of the flux intensities at 90° versus 0° were found to be 1.2 ± 0.2 . This finding likely indicates geometrical constraints of the decomposing complex, here a preferential hydrogen atom ejection parallel to the total angular momentum vector and perpendicularly to the plane defined by the rotating complex.³⁷ The above characteristics are also revealed in the flux contour map (Figure 4).

5. Discussion

First, let us summarize briefly the experimental findings before we discuss potential reaction mechanisms:

(1) A single product of mass-to-charge, $m/z = 27$, is formed. This has been assigned unambiguously to be a molecular of the empirical formula $^{11}\text{BNH}_2$. No molecular hydrogen elimination pathway is detectable.

(2) The reaction dynamics were found to be indirect. A transient complex living a significant fraction of a rotational period mediates the dynamics suggesting that the reactive system accesses the deep potential well associated with the formation of a $^{11}\text{BNH}_3$ intermediate. Cleavage of B–H or N–H bonds in that intermediate leads to BNH_2 and HBNH products, respectively.

(3) The kinetic energy release for product formation suggest that the reaction to form $^{11}\text{BNH}_2$ isomer(s) plus atomic hydrogen under single collision conditions is exoergic by $280 \pm 20 \text{ kJ mol}^{-1}$. The large kinetic energy release provides evidence that the more stable HBNH product is formed.

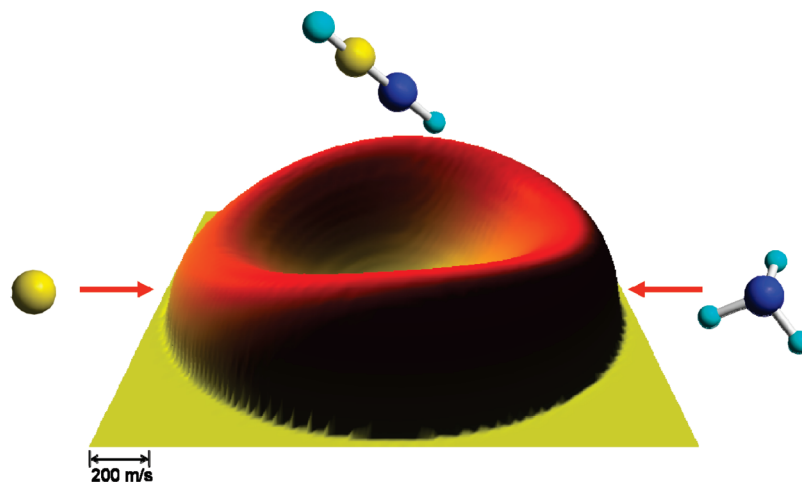


Figure 4. Flux contour map of the imidoborane molecule (HNBH) formed in the reaction of atomic boron, $^{11}\text{B}(^2\text{P}_j)$, with ammonia, $\text{NH}_3(\text{X}^1\text{A}_1)$, at a collision energy of 20.5 kJ mol^{-1} .

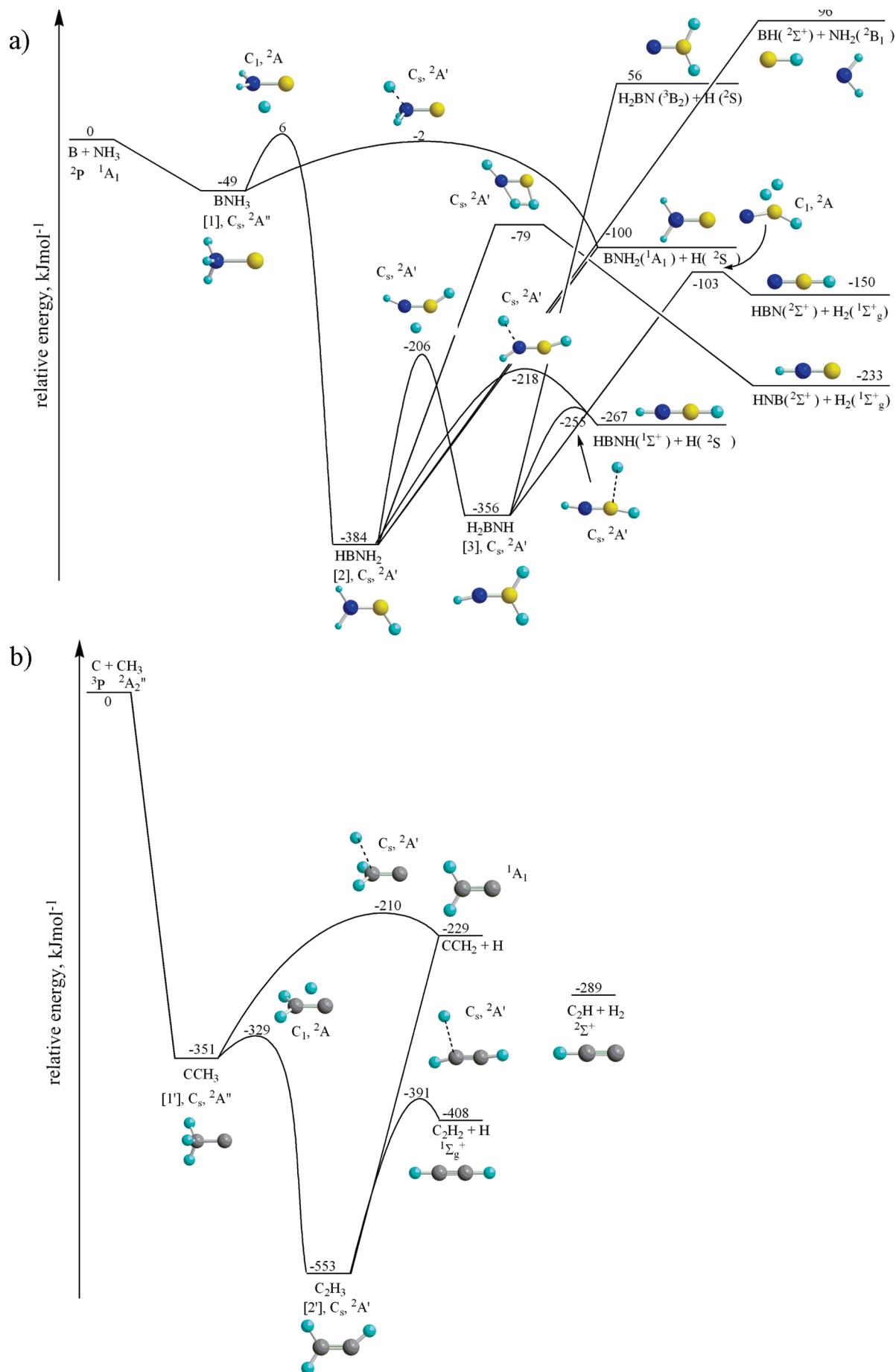


Figure 5. (a) Potential energy surfaces (PESs) of the isoelectronic boron-ammonia (top) and carbon-methyl (bottom) systems. (b) Potential energy surfaces (PESs) of the isoelectronic boron-ammonia (top) and carbon-methyl (bottom) systems.

Our electronic structure and intrinsic reaction coordinate (IRC) calculations indicate that the boron atom adds to the nonbonding electron-pair of the ammonia molecule without entrance barrier (Figure 5); this process forms the weakly bound, nearly C_{3v} symmetric BNH_3 intermediate [1]. The calculations suggest that this collision complex can either emit a hydrogen atom forming the C_{2v} symmetric BNH_2 product in an overall exoergic reaction of 100 kJ mol^{-1} with respect to the separated reactants or undergoes a hydrogen shift yielding the C_s symmetric HBNH_2 radical [2]. This radical fragments via molecular hydrogen loss to the linear HNB molecule and via atomic hydrogen loss to form HBNH ; this structure is 167 kJ mol^{-1} more stable than the BNH_2 isomer. This energy difference agrees nicely with an earlier theoretical study suggesting an energy difference of 173 kJ mol^{-1} .¹⁶ Alternatively, [2] isomerizes via hydrogen shift to the C_s symmetric H_2BNH radical [3]. This intermediate undergoes unimolecular decomposition via atomic or molecular hydrogen losses through tight exit transition states forming HBNH and HBN , respectively. Among the feasible H_2BN products, only the energetically highly unstable triplet H_2BN presents a local minimum; among all isomers in the triplet surface, triplet H_2BN holds the lowest energy.¹⁷ It should be stressed that a barrierless insertion of a boron atom into a nitrogen–hydrogen bond was not found computationally. To summarize, the electronic structure calculations indicate that two products can be formed via atomic and molecular hydrogen losses: HBNH and BNH_2 as well as HNB and HBN , respectively.

We are merging now these experimental findings with those obtained from electronic structure calculations to propose the actual reaction mechanism(s). These conclusions are then compared with the isoelectronic C_2H_3 and C_2H_2 potential energy surfaces. Our crossed beam experiments indicate that only the atomic, but no molecular hydrogen loss occurs. This can be readily understood in terms of the potential energy surface. Here, the barriers involved in the hypothetical formation of HNB and HBN of 305 and 253 kJ mol^{-1} , respectively, are higher compared to those required to pass in the atomic hydrogen loss from intermediates [2] and [3], that is, 284 (with no distinct transition state), 166, and 101 kJ mol^{-1} . On top of this, the decomposition of intermediate [3] thermodynamically favors the formation of HBNH versus HBN . Therefore, experiments and theory agree that the molecular hydrogen pathway is not present in the reaction dynamics of ground state boron atoms with ammonia. But what are the underlying chemical dynamics to form the BNH_2 isomer(s)? We propose that the boron atom adds to the lone electron pair of the ammonia molecule forming the BNH_3 intermediate via indirect scattering dynamics. Recall that the indirect scattering dynamics, that is, a reaction mechanism via the formation of a reaction intermediate/collision complex, was predicted based on the center-of-mass angular distributions and flux contour map (Figures 3 and 4). This collision complex undergoes one hydrogen migration to H_2BNH before this intermediate emits a hydrogen atom via a tight exit transition state forming the closed shell imidoborane molecule (HNBH). The experimental energetics of the formation of imidoborane plus atomic hydrogen of $280 \pm 20 \text{ kJ mol}^{-1}$ agree exceptionally well with the computed value of $267 \pm 5 \text{ kJ mol}^{-1}$. Also, the tight exit transition state was contemplated based on the off-zero peaking of the center-of-mass translational energy distribution. It is interesting to discuss the shape of the center-of-mass angular distribution in detail. The slightly higher intensity in the forward hemisphere indicates that the incorporated boron atom and leaving hydrogen atom must be incorporated on opposite sides of the rotational axis of the decomposing

complex. This is certainly fulfilled for intermediate [2], which was identified as a decomposing intermediate to form imidoborane. On the other hand, in intermediate [3], the boron atom and leaving hydrogen atom are on the same side of the rotational axis; therefore, a unimolecular decomposition of structure [3] cannot account for the experimentally found enhanced flux in the forward hemisphere of the center-of-mass angular distribution. Therefore, we can conclude that a comparison of the experimental and computational data suggest that at least the imidoborane molecule (HNBH) is formed via an initial addition of the electrophilic boron atom to ammonia followed by hydrogen migration and elimination via a tight exit transition state. It should be noted that besides HNBH , theory predicts that the BNH_2 molecule can be also produced in the reaction via a hydrogen atom loss from intermediate [1] or from structure [2]. According to our statistical calculations of rate constants for unimolecular reaction steps under single-collision conditions and at the experimental collision energy of 20.5 kJ mol^{-1} , the branching ratio of the BNH_2/HNBH products is expected to be about 3.6:1 if the system decomposes statistically.

6. Conclusions

From the chemical viewpoint, the concept of isoelectronic reactions plays an important role in the reaction of boron with ammonia once compared to bimolecular collisions of ground state carbon atoms with the methyl radical (CH_3). Here, both the B/NH_3 and isoelectronic C/CH_3 surfaces have no entrance barriers. Although the well depths of the initial collision complexes differ significantly from 49 to 351 kJ mol^{-1} , they can undergo hydrogen migration to vinyl (C_2H_3) and hydroimidoborane (HBNH_2) or form carbene-like structures (CCH_2 and BNH_2) in overall exoergic reactions. The intermediates can then also emit a hydrogen atom, forming the isoelectronic acetylene (HCCH) and imidoborane (HBNH) molecules both via tight exit transition states. Therefore, we can predict that, in the isoelectronic reaction of carbon atoms with the methyl radical, acetylene should be formed via a similar reaction mechanism (addition, hydrogen migration, and hydrogen elimination) as imidoborane. These conclusions show that crossed beam studies can be applied not only to study the formation of unstable transient species such as the imidoborane (HBNH) molecule, but also that the underlying mechanism can be utilized to predict the chemical reactivity of isoelectronic systems as demonstrated for the carbon-methyl radical—two open shell species—which are very difficult to study experimentally.

Acknowledgment. This work was supported by the Air Force Office of Scientific Research (A9550-09-1-0177) (F. Z., P. M., R. I. K.).

Supporting Information Available: Electronic structure calculation results. This information is free of charge via the Internet at <http://pubs.acs.org>.

References and Notes

- (1) Beachley, O. T., Jr. *J. Am. Chem. Soc.* **1970**, *92*, 5372.
- (2) Kiran, B.; Phukan, A. K.; Jemmis, E. D. *Inorg. Chem.* **2001**, *40*, 3615.
- (3) Fowler, P. W.; Steiner, E. *J. Phys. Chem. A* **1997**, *101*, 1409.
- (4) Allendorf, M. D.; Melius, C. F. *J. Phys. Chem. A* **1997**, *101*, 2670.
- (5) Lory, E. R.; Porter, R. F. *J. Am. Chem. Soc.* **1973**, *95*, 1766.
- (6) Kawashima, Y.; Kawaguchi, K.; Hirota, E. *J. Chem. Phys.* **1987**, *87*, 6331.
- (7) Thompson, C. A.; Andrews, L. *J. Am. Chem. Soc.* **1995**, *117*, 10125.
- (8) Thompson, C. A.; Andrews, L.; Martin, J. M. L.; El-Yazal, J. *J. Phys. Chem.* **1995**, *99*, 13839.

- (9) Wang, Z.-X.; Huang, M.-B.; Schleyer, P. v. R. *J. Phys. Chem. A* **1999**, *103*, 6475.
- (10) Barreto, P. R. P.; Vilela, A. F. A.; Gargano, R. *Int. J. Quantum Chem.* **2005**, *103*, 659.
- (11) Sharma, A. R.; Braams, B. J.; Carter, S.; Shepler, B. C.; Bowman, J. M. *J. Chem. Phys.* **2009**, *130*, 174301/1.
- (12) Hou, H.; Wang, B.; Gu, Y. *Phys. Chem. Chem. Phys.* **2000**, *2*, 5560.
- (13) Nielsen, I. M. B.; Janssen, C. L.; Burton, N. A.; Schaefer, H. F., III *J. Phys. Chem.* **1992**, *96*, 2490.
- (14) Smith, B. J.; Smernik, R.; Radom, L. *Chem. Phys. Lett.* **1992**, *188*, 589.
- (15) Osamura, Y.; Schaefer, H. F., III; Gray, S. K.; Miller, W. H. *J. Am. Chem. Soc.* **1981**, *103*, 1904.
- (16) Rosas-Garcia, V. M.; Crawford, T. D. *J. Chem. Phys.* **2003**, *119*, 10647.
- (17) Zhang, J.-G.; Li, Q. S.; Zhang, S.-W. *Int. J. Quantum Chem.* **2005**, *103*, 422.
- (18) Timoshkin, A. Y.; Schaefer, H. F., III *J. Phys. Chem. A* **2008**, *112*, 13180.
- (19) Gu, X.; Guo, Y.; Kawamura, E.; Kaiser, R. I. *J. Vac. Sci. Technol., A* **2006**, *24*, 505.
- (20) Guo, Y.; Gu, X.; Kawamura, E.; Kaiser, R. I. *Rev. Sci. Instrum.* **2006**, *77*, 034701/1.
- (21) Gu, X.; Guo, Y.; Zhang, F.; Mebel, A. M.; Kaiser, R. I. *Faraday Discuss.* **2006**, *133*, 245.
- (22) Vernon, M. *Molecular Beam Scattering*. Ph. D., University of California: Berkeley, 1981.
- (23) Weiss, P. S. *The Reaction Dynamics of Electronically Excited Alkali Atoms with Simple Molecules*. Ph. D., University Of California: Berkeley, 1986.
- (24) Raghavachari, K.; Trucks, G. W.; Pople, J. A.; Head-Gordon, M. *Chem. Phys. Lett.* **1989**, *157*, 479.
- (25) Bartlett, R. J.; Watts, J. D.; Kucharski, S. A.; Noga, J. *Chem. Phys. Lett.* **1990**, *165*, 513.
- (26) Gauss, J.; Lauderdale, W. J.; Stanton, J. F.; Watts, J. D.; Bartlett, R. J. *Chem. Phys. Lett.* **1991**, *182*, 207.
- (27) Watts, J. D.; Gauss, J.; Bartlett, R. J. *J. Chem. Phys.* **1993**, *98*, 8718.
- (28) Dunning, T. H., Jr. *J. Chem. Phys.* **1989**, *90*, 1007.
- (29) Stanton, J. F.; Gauss, J.; Perera, S. A.; Yau, A. D.; Watts, J. D.; Nooijen, M.; Oliphant, N.; Szalay, P. G.; Lauderdale, W. J.; Gwaltney, S. R.; Beck, S.; Balkova', A.; Bernholdt, D. E.; Baeck, K.-K.; Rozycko, P.; Sekino, H.; Huber, C.; Pittner, J.; Bartlett, R. J. *Aces II, Quantum Theory Project*; University of Florida: Gainesville, FL. Integral packages included are: Almlöf, J.; Taylor, P. R. VMOL; Taylor, P. R. VPROPS; and Helgaker, T.; Aa. Jensen, H. J.; Jorgensen, P.; Olsen, J.; Taylor, P. R. ABACUS.
- (30) Frisch, M. J.; Trucks, G. W.; Schlegel, H. B.; Scuseria, G. E.; Robb, M. A.; Cheeseman, J. R.; Zakrzewski, V. G.; J. A. Montgomery, J.; Stratmann, R. E.; Burant, J. C.; Dapprich, S.; Millam, J. M.; Daniels, A. D.; Kudin, K. N.; Strain, M. C.; Farkas, O.; Tomasi, J.; Barone, V.; Cossi, M.; Cammi, R.; Mennucci, B.; Pomelli, C.; Adamo, C.; Clifford, S.; Ochterski, J.; Petersson, G. A.; Ayala, P. Y.; Cui, Q.; Morokuma, K.; Malick, D. K.; Rabuck, A. D.; Raghavachari, K.; Foresman, J. B.; Cioslowski, J.; Ortiz, J. V.; Baboul, A. G.; Stefanov, B. B. G.; Liu, A. L.; Piskorz, P.; Komaromi, I.; Gomperts, R.; Martin, R. L.; Fox, D. J.; Keith, T.; Al-Laham, M. A.; Peng, C. Y.; Nanayakkara, A.; Gonzalez, C.; Challacombe, M.; Gill, P. M. W.; Johnson, B. G.; Chen, W.; Wong, M. W.; Andres, J. L.; Head-Gordon, M.; Replogle, E. S.; Pople, J. A. *Gaussian 98*, Revision A5; Gaussian, Inc.: Pittsburgh PA, 1998.
- (31) Amos R. D., Bernhardsson A., Berning A., Celani P., Cooper D. L., Deegan M. J. O., Dobbyn A. J., Eckert F., Hampel C., Hetzer G., Knowles P. J., Korona T., Lindh R., Lloyd A. W., McNicholas S. J., Manby F. R., Meyer W., Mura M. E., Nicklass A., Palmieri P., Pitzer R., Rauhut G., Schutz M., Schumann U., Stoll H., Stone A. J., Tarroni R., Thorsteinsson T., Werner H.-J. *MOLPRO, version 2002 6, a package of ab initio programs*; 2002; See <http://www.molpro.net>.
- (32) Kaiser, R. I. *Chem. Rev.* **2002**, *102*, 1309.
- (33) Guo, Y.; Gu, X.; Zhang, F.; Sun, B. J.; Tsai, M. F.; Chang, A. H. H.; Kaiser, R. I. *J. Phys. Chem. A* **2007**, *111*, 3241.
- (34) Kaiser, R. I.; Mebel, A. M. *Int. Rev. Phys. Chem.* **2002**, *21*, 307.
- (35) Bullitt, M. K.; Fisher, C. H.; Kinsey, J. L. *J. Chem. Phys.* **1974**, *60*, 478.
- (36) Kaiser, R. I.; Oschensfeld, C.; Head-Gordon, M.; Lee, Y. T.; Suits, A. G. *Science* **1996**, *274*, 1508.
- (37) Bettinger, H. F.; Kaiser, R. I. *J. Phys. Chem. A* **2004**, *108*, 4576.